INDIAN JOURNAL OF SCIENCE AND TECHNOLOGY

ORIGINAL ARTICLE

Check for updates

MHD Flow of Cu–Al_2O_3/Water Hybrid Nanofluid past a Porous Wedge with Variable Fluid Properties and Convective Boundary Condition

Mwblib Basumatary[1]*

1 Department of Mathematics, Lumding College, Lumding-782447, Assam, India

OPEN ACCESS

Received: 29/09/2025

Accepted: 11/10/2025

Published: 29/10/2025

Citation: Basumatary M (2025) MHD Flow of Cu–Al_2O_3/Water Hybrid Nanofluid past a Porous Wedge with Variable Fluid Properties and Convective Boundary Condition. Indian Journal of Science and Technology 18(40): 3198-3208. https://doi.org/10.17485/IJST/v18i40.1607

* **Corresponding author**.

mwblib.lmg@gmail.com

Funding: None

Competing Interests: None

Published By Indian Society for Education and Environment (iSee)

ISSN
Print: 0974-6846
Electronic: 0974-5645

Abstract

Objective: The present study investigates the magnetohydrodynamic (MHD) boundary layer flow and thermal transport behavior of a Cu–Al_2O_3/water hybrid nanofluid past a porous wedge with convective boundary condition. Both viscosity and thermal conductivity are considered as functions of temperature to account for variable fluid properties, while thermal radiation and local buoyancy effects are included to model mixed convection. **Method:** Using appropriate similarity transformations, the system of partial differential equations governing mass, momentum, and energy is converted into nonlinear ordinary differential equations (ODEs) and tackled numerically through MATLAB's bvp4c routine. Variations in thermal radiation, viscosity, thermal conductivity, and magnetic field strength are thoroughly examined to assess their role in velocity, temperature, skin friction, and heat transfer characteristics, and the results are presented graphically. **Findings:** The current results are compared with earlier studies and found a strong agreement in some specific cases. Increasing the variable viscosity parameter (θ_r) from $-\infty$ (constant case) to -2, -0.5, -0.1 and -0.05 reduces the skin friction coefficient by 27.79%, 56.91%, 81.83% and 87.86%, respectively, thereby improving the velocity profile. However, the local Nusselt number increases by 1.34%, 4.53%, 13.29% and 18.37%, which corresponds to a decrease in the temperature profile. The variable thermal conductivity parameter (θ_s) increases the fluid temperature when radiation or Biot number act individually. In contrast, under their combined influence, higher θ_s promotes heat dissipation, thereby decreasing the fluid temperature. **Novelty:** This work provides an innovative investigation into the effects of variable viscosity and thermal conductivity on MHD flow of hybrid nanofluid past a porous wedge under convective boundary condition and thermal radiation, a topic that has not yet been reported in existing literature. The proposed formulation offers a novel, unified framework for predicting more accurately the thermofluids behavior in advanced thermal management and energy system applications.

Keywords: Hybrid nanofluid; Variable properties; Porous wedge; MHD flow; Similarity transformation

1 Introduction

Hybrid nanofluids, consisting of two or more distinct types of nanoparticles suspended in a base fluid, have emerged as a highly promising class of heat transfer fluids. In comparison to conventional single-component nanofluids, hybrid nanofluids exhibit significantly enhanced thermal conductivity, improved stability, and superior heat transfer efficiency[1]. These advantageous properties make hybrid nanofluids highly attractive for numerous engineering and industrial applications, including solar energy systems, refrigeration, heating, air conditioning, ventilation, thermal exchangers, heated pipes, electronics cooling, automotive systems, biomedical applications, aerospace technology, marine engineering, and defense mechanisms[2]. Recent studies have focused on boundary layer flows over wedge surfaces involving hybrid nanofluids. Zainal et al.[3] investigated unsteady hybrid nanofluid flow over a moving Falkner–Skan wedge and showed that dual-type nanoparticles and wedge angle parameters enhance thermal efficiency. Alqahtani et al.[4] numerically examined hybrid nanofluid flow and stability over a porous wedge, providing insights into fluid dynamics and heat transfer under porous conditions. Furthermore, Panda et al.[5] analyzed buoyancy-driven dissipative Falkner–Skan flow of hybrid nanofluids over a vertical permeable wedge, emphasizing the mechanisms of heat transfer in such systems.

Magnetohydrodynamic (MHD) flow has been extensively examined within the framework of hybrid nanofluids due to its ability to control electrically conducting fluids and improve thermal transport. Sharma et al.[6] and Mathews and Hymavathi[7] studied MHD stagnation-point flow and heat transfer by considering Cu–Al_2O_3/ethylene glycol and Al_2O_3–Cu/water hybrid nanofluids, respectively. Their numerical results demonstrated that the combined effects of magnetic fields and hybrid nanoparticles markedly enhance heat transfer. Ahmed[8] explored the effect of variable electrical conductivity on MHD hybrid nanofluid flow through an annular sector duct. Furthermore, Alshehry et al.[9] have examined hybrid nanofluid transport cone and over wedge geometries under magnetic fields, further confirming the significance of MHD in improving both flow and thermal performance across diverse configurations.

Convective boundary conditions have received increasing attention in wedge- and stretching-surface problems due to their more realistic representation of surface heat exchange. Yahaya et al.[10] reported that convective boundary conditions enhance heat transfer and influence solution stability in mixed convection hybrid nanofluid flow over a cone and wedge. Further, Pattnaik et al.[11] and Ogunniyi et al.[12] confirmed that in MHD hybrid nanofluids, the convective parameter regulates how magnetic effects translate into changes in wall temperature and local Nusselt number.

Recent studies have focused on the influence of temperature-dependent fluid properties. However, most of the previous works have considered these properties as constant. Since the variations in viscosity and thermal conductivity play crucial role in determining the momentum and heat transfer characteristics of the fluid so, it is necessary to consider these properties as functions of temperature. Mandal and Pal[13] have taken variable viscosity and thermal conductivity into account and presented double solutions and stability sensitivity for Ag–MoS_2/water nanofluids over a Riga surface. In the same vein, Rafique et al.[14] pointed out that such variable properties appreciably alter temperature profiles, Nusselt number in radiative and Joule-heated wedge flows. More recently, Abbas et al.[15] investigated the flow and heat transfer characteristics of a Cu–Al_2O_3/H_2O hybrid nanofluid over a porous stretching sheet by considering temperature dependent viscosity and viscous dissipation effects. Their findings revealed that raising temperature reduces viscosity by approximately 21.3%, resulting in a rise in the velocity profile and weakening the momentum boundary layer.

This study is conducted to examine the MHD flow of a Cu–Al_2O_3/water hybrid nanofluid past a porous wedge, incorporating variable fluid properties, thermal radiation, local buoyancy effects, and a convective boundary condition. Unlike previous studies that considered only one or two of these factors individually, the present work examines all these effects simultaneously, providing a more comprehensive and realistic analysis of hybrid nanofluid heat transfer for practical engineering applications.

2 Methodology

Let us now consider a steady, laminar, two-dimensional boundary-layer flow of an incompressible viscous Cu–Al_2O_3/water hybrid nanofluid past a stationary wedge. The x-axis is taken along the surface of the wedge, and the y-axis is perpendicular to it as shown in Figure 1. Here, the ambient velocity is given by $U(x) = U_\infty\, x^m$, where U_∞ and m are constants. A magnetic field $B(x) = B_0\, x^{(m-1)/2}$ is applied along y-direction, where B_0 is a constant. The magnetic Reynolds number is assumed to be small so that the induced magnetic field is neglected. The wedge surface is convectively heated by a hot hybrid nanofluid at temperature T_f with heat transfer coefficient h_f. In addition, the wedge is assumed to be porous with mass transfer velocity V_w, where $V_w > 0$ corresponds to mass injection, $V_w < 0$ indicates mass suction and $V_w = 0$ denotes an impermeable surface.

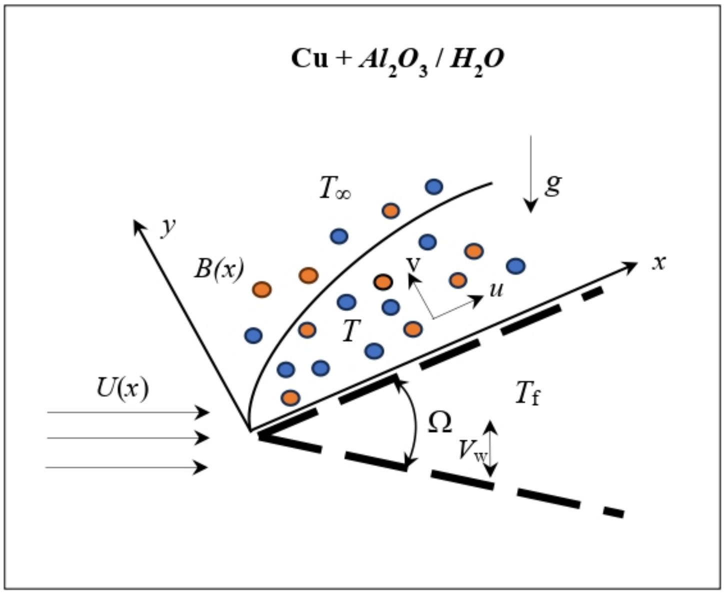

Fig 1. Geometry of the flow system

Based on the above assumptions and following Parida et al.[16] and Anuar et al.[17], the governing equations for the hybrid nanofluid are

$$\frac{\partial u}{\partial x}+\frac{\partial v}{\partial y}=0 \tag{1}$$

$$\begin{aligned}\rho_{hnf}\left(u\frac{\partial u}{\partial x}+v\frac{\partial u}{\partial y}\right) &= \rho_{hnf}U\frac{\mathrm{dU}}{dx}+\frac{\partial}{\partial y}\left(\mu^*_{hnf}\frac{\partial u}{\partial y}\right)\\ &+(\rho\beta_T)_{hnf}\,g\,(T-T_\infty)\sin(\Omega/2)-\sigma_{hnf}\,B^2(x)(u-U)\end{aligned} \tag{2}$$

$$(\rho C_p)_{hnf}\left(u\frac{\partial T}{\partial x}+v\frac{\partial T}{\partial y}\right)=\frac{\partial}{\partial y}\left(K^*_{hnf}\frac{\partial T}{\partial y}\right)-\frac{\partial q_r}{\partial y} \tag{3}$$

and the boundary conditions are

$$\left.\begin{aligned} u&=0,\ \mathrm{v}=V_w,\ -K^*_{\mathrm{hnf}}\frac{\partial T}{\partial y}=h_f\left(T_f-T\right)\ \text{at}\ y=0\\ u&=U(x),\ T=T_\infty\ \text{as}\ y\to\infty\end{aligned}\right\} \tag{4}$$

Here, *u* and v represent velocity components along the *x*- and *y*- axes, respectively; and *g* is acceleration due to gravity.

The radiative heat flux q_r (using Rosseland approximation) is defined as[18]:

$$q_r=-\frac{4\sigma^*}{3k^*}\frac{\partial T^4}{\partial y} \tag{5}$$

where k^* represents the absorption coefficient of the medium and σ^* stands the Stefan-Boltzmann constant. To simplify the nonlinear term T^4, a Taylor series expansion at T_∞ is used. By discarding higher order terms, the expression reduces to:

$$T^4\approx 4{T_\infty}^3T-3{T_\infty}^4 \tag{6}$$

Substituting equation (6) into equation (5) and differentiating with respect to y, the radiative heat flux gradient becomes:

$$\frac{\partial q_r}{\partial y}=-\frac{16\sigma^*{T_\infty}^3}{3k^*}\frac{\partial^2 T}{\partial y^2} \tag{7}$$

2.1 Variable Viscosity (μ^*_{hnf})

$$\mu^*_{hnf} = \mu_{hnf}\frac{\mu_f(T)}{\mu_{H_2O}}$$

$$\text{where } \mu_{hnf} = \frac{\mu_{H_2O}}{(1-\phi_{Cu})^{2.5}(1-\phi_{Al_2O_3})^{2.5}} \text{ and } \mu_f(T) = \frac{\mu_{H_2O}}{[1+\gamma(T-T_\infty)]} \tag{8}$$

Here, ϕ_{Cu} and $\phi_{Al_2O_3}$ are the solid volume fractions of Cu and Al_2O_3 nanoparticles.

2.2 Density

$$\rho_{hnf} = \phi_{Cu}\rho_{Cu} + \left[(1-\phi_{Cu})\left\{\left(1-\phi_{Al_2O_3}\right)\rho_{H_2O} + \phi_{Al_2O_3}\rho_{Al_2O_3}\right\}\right]$$

where $\rho_{H_2O} = 997.1 kg.m^{-3}, \rho_{Cu} = 8933 kg.m^{-3}$ and $\rho_{Al_2O_3} = 3970 kg.m^{-3}$ [19]

2.3 Specific Heat

$$(\rho C_p)_{hnf} = \phi_{Cu}(\rho C_p)_{Cu} + \left[(1-\phi_{Cu})\left\{\begin{array}{c}\left(1-\phi_{Al_2O_3}\right)(\rho C_p)_{H_2O}\\ +\phi_{Al_2O_3}(\rho C_p)_{Al_2O_3}\end{array}\right\}\right]$$

where $(C_p)_{H_2O} = 4179 J.kg^{-1}.K^{-1}, (C_p)_{Cu} = 385 J.kg^{-1}.K^{-1}, (C_p)_{Al_2O_3} = 765 J.kg^{-1}.K^{-1}$ [20].

2.4 Variable Thermal Conductivity

$$\begin{aligned}
K^*_{hnf} &= K_{hnf}\frac{K_f(T)}{K_{H_2O}}\\
\text{where } K_{\text{hnf}} &= K_{nf}\frac{[K_{Cu}+2K_{nf}-2\phi_{Cu}(K_{nf}-K_{Cu})]}{[K_{Cu}+2K_{nf}+\phi_{Cu}(K_{nf}-K_{Cu})]},\\
K_{\text{nf}} &= K_{H_2O}\frac{\left[K_{Al_2O_3}+2K_{H_2O}-2\phi_{Al_2O_3}\left(K_{H_2O}-K_{Al_2O_3}\right)\right]}{\left[K_{Al_2O_3}+2K_{H_2O}+\phi_{Al_2O_3}\left(K_{H_2O}-K_{Al_2O_3}\right)\right]}\\
\text{and } K_f(T) &= K_{H_2O}[1+\delta(T-T_\infty)]
\end{aligned} \tag{9}$$

Here, $K_{H_2O} = 0.613 Wm^{-1}K^{-1}, K_{Cu} = 401 Wm^{-1}K^{-1}$ and $K_{Al_2O_3} = 40 Wm^{-1}K^{-1}$ [20].

2.5 Electrical Conductivity

$$\sigma_{hnf} = \sigma_{nf}\frac{[\sigma_{Cu}+2\sigma_{nf}-2\phi_{Cu}(\sigma_{nf}-\sigma_{Cu})]}{[\sigma_{Cu}+2\sigma_{nf}+\phi_{Cu}(\sigma_{nf}-\sigma_{Cu})]}$$

$$\sigma_{nf} = \sigma_{H_2O}\frac{\left[\sigma_{Al_2O_3}+2\sigma_{H_2O}-2\phi_{Al_2O_3}\left(\sigma_{H_2O}-\sigma_{Al_2O_3}\right)\right]}{\left[\sigma_{Al_2O_3}+2\sigma_{H_2O}+\phi_{Al_2O_3}\left(\sigma_{H_2O}-\sigma_{Al_2O_3}\right)\right]}$$

where $\sigma_{H_2O} = 5.5\times10^{-6} S.m^{-1}, \sigma_{Cu} = 59.6\times10^{6} S.m^{-1}, \sigma_{Al_2O_3} = 1\times10^{-10} S.m^{-1}$ [20].

2.6 Thermal Expansion Coefficient

$$(\rho\beta_T)_{\text{hnf}} = \phi_{Cu}(\rho\beta_T)_{Cu} + \left[(1-\phi_{Cu})\left\{\left(1-\varphi_{Al_2O_3}\right)(\rho\beta_T)_{H_2O} + \phi_{Al_2O_3}(\rho\beta_T)_{Al_2O_3}\right\}\right]$$

where $(\beta_T)_{H_2O} = 21\times10^{-5}.K^{-1}, (\beta_T)_{Cu} = 1.67\times10^{-5}.K^{-1}, (\beta_T)_{Al_2O_3} = 0.63\times10^{-5}.K^{-1}$ [19].

To solve the governing equations (1)–(3) along with the boundary conditions (4), the following dimensionless similarity transformations are employed

$$\left.\psi = \left[\frac{2\nu_{H_2O}xU}{(m+1)}\right]^{1/2} f(\eta), \eta = y\left[\frac{(m+1)U}{\left(2\nu_{H_2O}x\right)}\right]^{1/2}, \theta(\eta) = \frac{(T-T_\infty)}{(T_f-T_\infty)}\right\} \tag{10}$$

where ψ is the stream function defined by $u = \partial\psi/\partial y$ and $v = -\partial\psi/\partial x$ which satisfies equation (1) and ν_{H_2O} is the kinematic viscosity of water. Additionally, we define the variable viscosity parameter as:

$$\theta_r = -\frac{1}{\gamma(T_f-T_\infty)} \tag{11}$$

Physically, the viscosity of liquids, including hybrid nanofluids, typically decreases with increasing temperature. As a result, θ_r takes negative values for hybrid nanofluids.

Under these transformations, the equations (2) and (3) are converted to the following similarity equations:

$$\begin{aligned} &A_1\left[\frac{f'''}{(1-\theta/\theta_r)} + \frac{f''\theta'}{\theta_r(1-\theta/\theta_r)^2}\right] + A_2\left[ff'' + \beta\left(1-f'^2\right)\right] \\ &+ A_3(2-\beta)\lambda\sin(\Omega/2)\theta - A_4(2-\beta)M(f'-1) = 0 \end{aligned} \tag{12}$$

$$\frac{1}{\mathrm{Pr}_{H_2O}}\left[\left\{A_6(1+\theta_s\theta) + \frac{4}{3}R\right\}\theta'' + \theta_s A_6(\theta')^2\right] + A_5 f\theta' = 0 \tag{13}$$

$$\left.\begin{aligned} \text{where } A_1 = \frac{\mu_{hnf}}{\mu_{H_2O}},\ A_2 = \frac{\rho_{hnf}}{\rho_{H_2O}},\ A_3 = \frac{(\rho\beta_T)_{hnf}}{(\rho\beta_T)_{H_2O}} \\ A_4 = \frac{\sigma_{hnf}}{\sigma_{H_2O}},\ A_5 = \frac{(\rho C_p)_{hnf}}{(\rho C_p)_{H_2O}},\ A_6 = \frac{K_{hnf}}{K_{H_2O}} \end{aligned}\right\} \tag{14}$$

The transformed boundary conditions (4) are

$$\left.\begin{aligned} f(0) = f_w, f'(0) = 0, \theta'(0) = \frac{Bi\sqrt{(2-\beta)}\left[\theta(0)-1\right]}{A_6\left[1+\theta_s\theta(0)\right]} \\ f'(\infty) =, \theta(\infty) = 0 \end{aligned}\right\} \tag{15}$$

where the prime symbol ($'$) denotes differentiation with respect to η. The dimensionless pressure gradient parameter β = $2m/(m+1)$ corresponds the Hartree parameter and is related to wedge angle Ω as $\beta = \Omega/\pi$.

Suction/injection parameter f_w, variable thermal conductivity parameter, the Grashof number Gr_x, Reynolds number Re_x, local buoyancy parameter Λ, magnetic parameter M, radiation parameter R, constant Prandtl number Pr_{H_2O} and Biot number Bi are defined as

$$\left.\begin{aligned} f_w = -V_w\left[\frac{2x}{(m+1)\upsilon_{H_2O}U}\right]^{1/2}, \theta_s = \delta(T_f-T_\infty), \\ Gr_x = \frac{g(\beta_T)_{H_2O}(T_f-T_\infty)x^3}{\upsilon_{H_2O}}, Re_x = \frac{xU}{\upsilon_{H_2O}}, \Lambda = \frac{Gr_x}{Re_x^{1/2}}, M = \frac{\sigma_{H_2O}B_0^2}{\rho_{H_2O}U_\infty}, \\ R = \frac{4K_{H_2O}\sigma^*{T_\infty}^3(T_f-T_\infty)}{k^*}, Pr_{H_2O} = \frac{\mu_{H_2O}(C_p)_{H_2O}}{K_{H_2O}},\ Bi = \frac{h_f\,x}{K_{H_2O}Re_x^{1/2}} \end{aligned}\right\} \tag{16}$$

The flow is assisting for $\Lambda > 0$, opposing for $\Lambda < 0$ and reduces to forced convection when $\Lambda = 0$.

The variable Prandtl number is defined as:

$$Pr = \frac{\mu_f(T)\ (C_p)_{H_2O}}{K_f(T)} = \frac{Pr_{H_2O}}{(1-\theta/\theta_r)(1+\theta_s\theta)} \tag{17}$$

By using **equation (17)**, the **equation (13)** can be expressed as

$$\frac{1}{\Pr(1-\theta/\theta_r)(1+\theta_s\theta)}\left[\left\{A_6(1+\theta_s\theta)+\frac{4}{3}R\right\}\theta''+A_6\theta_s(\theta')^2\right]+A_5 f\theta'=0 \tag{18}$$

Finally, the expressions for the local skin-friction coefficient (C_f) and the local Nusselt number (*Nu*) are given by the following relations:

$$C_f = \frac{2}{\rho_{H_2O}U^2}\left(\mu^*_{hnf}\frac{\partial u}{\partial y}\right)_{y=0} \text{ and } Nu = -\frac{x}{K_{H_2O}(T_f-T_\infty)}\left[K^*_{hnf}\frac{\partial T}{\partial y}-q_r\right]_{y=0} \tag{19}$$

Using (10), the quantities of (19) can be written as follows:

$$Re_x{}^{1/2}C_f = \frac{2A_1}{(2-\beta)^{1/2}(1-1/\theta_r)}f''(0) \tag{20}$$

$$Re_x{}^{-1/2}Nu_x = -\frac{1}{(2-\beta)^{1/2}}\left[A_6(1+\theta_s)+\frac{4}{3}R\right]\theta'(0) \tag{21}$$

2.7 Method of Numerical Solution

In this study, the boundary value problems presented in **Equations (12) and (18)**, together with the associated boundary conditions specified in **Equation (15)**, are numerically solved using the procedure outlined by Prasad et al.[21], with MATLAB's built-in solver bvp4c. For computational purposes, the similarity variable η is considered over the finite interval [0, 5] rather than the infinite domain $[0, \infty)$. A uniform step size of h = 0.05 and an error tolerance of 10^{-6} were used to achieve numerical accuracy.

3 Results and Discussion

This section presents a detailed investigation of the steady incompressible flow of a MHD Cu–Al_2O_3/water hybrid nanofluid past a porous wedge under convective boundary condition, considering temperature-dependent viscosity and thermal conductivity. The MATLAB's bvp4c function is used to obtain numerical solutions. A systematic analysis is conducted to evaluate the effects of key parameters on the velocity and temperature fields, as well as on the local skin friction coefficient and Nusselt number. The numerical results are presented through tables and MATLAB-generated figures, accompanied by a discussion of their physical significance using default parameter values $\beta = 1/3$, Pr = 6.2, $\theta_r = -0.5$, θ_s = fw = Bi = 0.5, M = Λ = R = 1, $\phi_{Cu} = \phi_{Al_2O_3} = 0.01$, unless otherwise stated.

To verify the validity of the proposed method, the quantities $f''(0)$ and $-\theta'(0)$ were computed for various values of *m* under the limiting case Pr = 0.73, $\theta_r \to \infty$, $\phi_{Cu} = \phi_{Al_2O_3} = \Lambda = M = f_w = R = \theta_s = 0$ and $Bi \to \infty$. The obtained results were then compared with the established results reported by Ibrahim & Tulu[22], as shown in Table 1. The data presented in the table demonstrates excellent agreement, thereby confirming the accuracy of the proposed numerical approach.

Table 2 is presented to elucidate the role of the Cu–Al_2O_3/water hybrid nanofluid on the local skin friction coefficient $Re_x{}^{1/2} C_f$ and the local Nusselt number $Re_x{}^{-1/2}$ *Nu* for four cases (i) without radiation and Biot number, (ii) with radiation only, (iii) with Biot number only, and (iv) with both radiation and Biot number. The result shows that the existence of the hybrid nanofluid raises the local skin friction coefficient in all the cases, typically due to its higher effective viscosity and enhanced momentum diffusion compared with the mono nanofluid. Regarding heat transfer, the hybrid nanofluid helps an increase in the local Nusselt number when either radiation or Biot number acts individually, as observed in cases (i)–(iii). The observed augmentation is due to the improved effective thermal conductivity of the hybrid nanofluid, which strengthens the wall heat exchange. However, under the combined effect of radiation and Biot number (case iv), radiative energy transport and surface convection reduce

Table 1. Comparison of results for $f''(0)$ and $-\theta'(0)$ for various values of m at Pr = 0.73, $\theta_r \to \infty$, $Bi \to \infty$ with other parameters zero

m	$f''(0)$		$-\theta'(0)$	
	Ibrahim & Tulu [22]	Present work	Ibrahim & Tulu [22]	Present work
0.0000	0.46960	0.469601	0.42016	0.420160
0.0141	0.50461	0.504615	0.42578	0.425784
0.0435	0.56898	0.568978	0.43548	0.435482
0.0909	0.65498	0.654980	0.44730	0.447303
0.1429	0.73200	0.731999	0.45694	0.456939
0.2000	0.80213	0.802126	0.46503	0.465034
0.3333	0.92765	0.927654	0.47814	0.478139
1.0000	1.23280	1.232588		0.504182

Table 2. Effect of the hybrid nanofluid on local skin friction coefficient $\mathrm{Re}_x{}^{1/2}C_f$ and the local Nusselt number $\mathrm{Re}_x{}^{-1/2}\,Nu$

ϕ_{Cu}	R	Bi	$\mathrm{Re}_x{}^{1/2}C_f$	$\mathrm{Re}_x{}^{-1/2}\,Nu$
0.00	0	∞	2.351247	6.734354
0.01			2.504053	6.749146
0.02			2.664724	6.764173
0.00	1	∞	2.297521	7.419104
0.01			2.447712	7.434814
0.02			2.605781	7.450299
0.00	0	0.5	1.132081	0.607526
0.01			1.208321	0.607942
0.02			1.288582	0.608361
0.00	1	0.5	1.231841	0.996071
0.01			1.311212	0.987138
0.02			1.394659	0.987138

the wall temperature gradient by thickening the thermal boundary layer, leading to a decline in heat transfer rate despite the improved conductivity of the hybrid nanofluid.

The effect of the magnetic parameter M on the velocity and temperature distributions of Cu-Al_2O_3/water hybrid nanofluid is presented in Figure 2(a)—(b). It is observed that increasing magnetic parameter (M) enhances the hybrid nanofluid fluid velocity, while the temperature profile decreases. The MHD term in equation (2), given by $-\sigma_{hnf}\,B^2\,(x)\,(u{-}U)$, incorporates the effects of the Lorentz force that resists fluid motion, and an external force arising from the interaction of the magnetic field and the free stream velocity, which promotes fluid motion. Within the boundary layer, where $u < U$, this term becomes positive, indicating that the external force surpasses the opposing Lorentz force and acts as a forcing term for the flow. As M increases, the magnitude of this net forcing term also increases, thereby enhancing fluid acceleration within the boundary layer. Thus, the magnetic field reduces flow resistance and promotes faster fluid motion. This enhanced motion improves convective heat transfer from the wedge surface, causing a reduction in the hybrid nanofluid temperature. Consequently, both boundary layer thicknesses become thinner as M increases.

Figure 3(a)—(b) illustrate how the variable viscosity parameter θ_r affects the velocity and temperature profiles of Cu—Al_2O_3/water hybrid nanofluid. It is clearly seen that decreasing $|\theta_r|$ increases the velocity profile while reducing the temperature profile. Physically, a smaller value of $|\theta_r|$ corresponds to higher temperature difference between the wedge surface and the fluid, which weakens viscosity and reduces flow resistance, thereby growing hybrid nanofluid velocity. On the other hand, the thermal boundary layer becomes thinner with decreasing $|\theta_r|$, which lowers the wall temperature and reduces the rate of heat transfer.

To investigate the impact of θ_s on the fluid temperature, we plot Figure 4(a) for four different cases (i) without Biot number and radiation, (ii) with radiation only, (iii) with Biot number only, and (iv) with both radiation and Biot number. The temperature of hybrid nanofluid increases with the augmented values of θ_s in the first three cases: (i), (ii) and (iii). It can be explained that the higher thermal conductivity enhances the fluid's capability to transfer and store heat, either by conduction or by distributing energy gained from surface convection or radiation. In contrast, for case (iv), the fluid temperature decreases

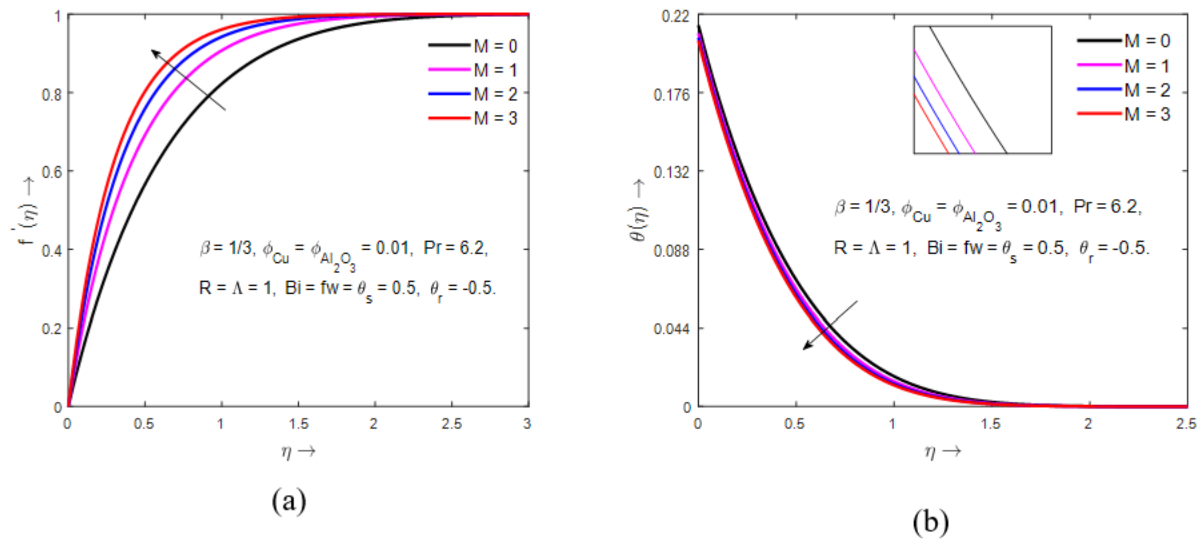

Fig 2. Velocity and temperature profiles with respect to M

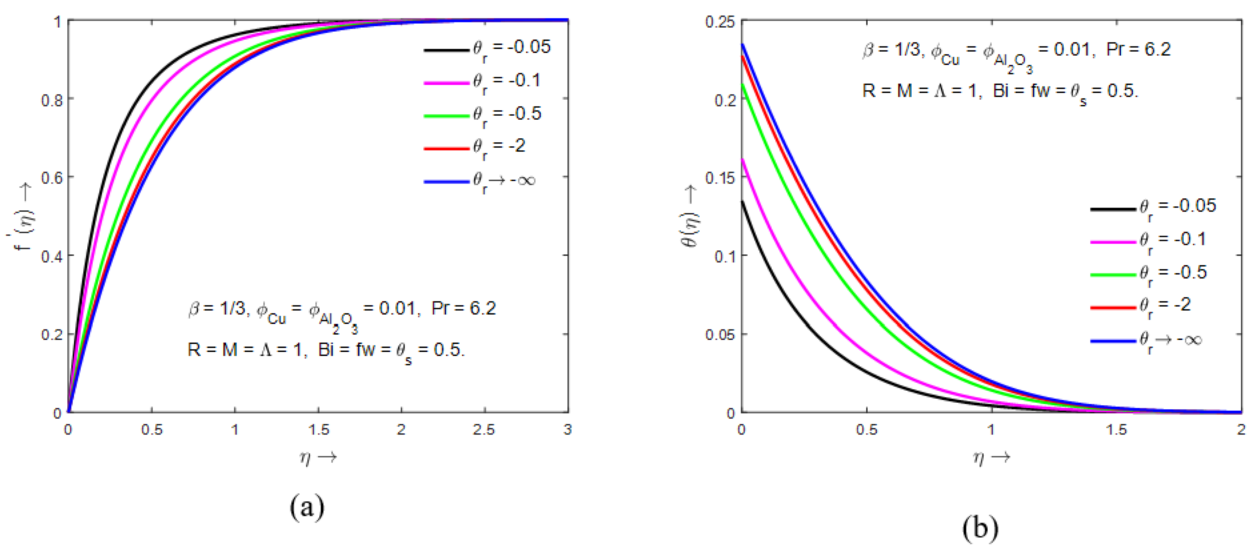

Fig 3. Velocity and temperature profiles with respect to θ_r.

with increasing θ_s. This is because the combined effect of surface convection and radiation promotes heat dissipation, and higher thermal conductivity facilitates more effective transfer of heat away from the hybrid nanofluid near the wedge, resulting in a net reduction in temperature. The temperature profiles exhibit an enhancement with an escalation in radiation parameter, as illustrated in Figure 4(b).

Figure 5(a)—(b) demonstrate that both $\mathrm{Re}_x{}^{1/2}C_f$ and $\mathrm{Re}_x{}^{-1/2}Nu$ rise with increasing M and f_w, regardless of whether viscosity is constant ($\theta_r \to \infty$) or variable ($\theta_r = -0.5$). This is due to the Lorentz force formed by the magnetic field, which resists the fluid motion and fortifies the velocity gradient at the wall, thereby increasing the skin friction coefficient. At the same time, the magnetic damping effect suppresses fluid motion within the boundary layer, resulting in a reduced thermal boundary layer along with a sharper wall temperature gradient, which enhances heat transfer. Similarly, wall suction reduces both the velocity and thermal boundary layers thicknesses by drawing hybrid nanofluid motion toward the wedge surface, thereby sharpening the shear and thermal gradients. Consequently, this mechanism leads to higher values of both $\mathrm{Re}_x{}^{1/2}C_f$ and $\mathrm{Re}_x{}^{-1/2}Nu$.

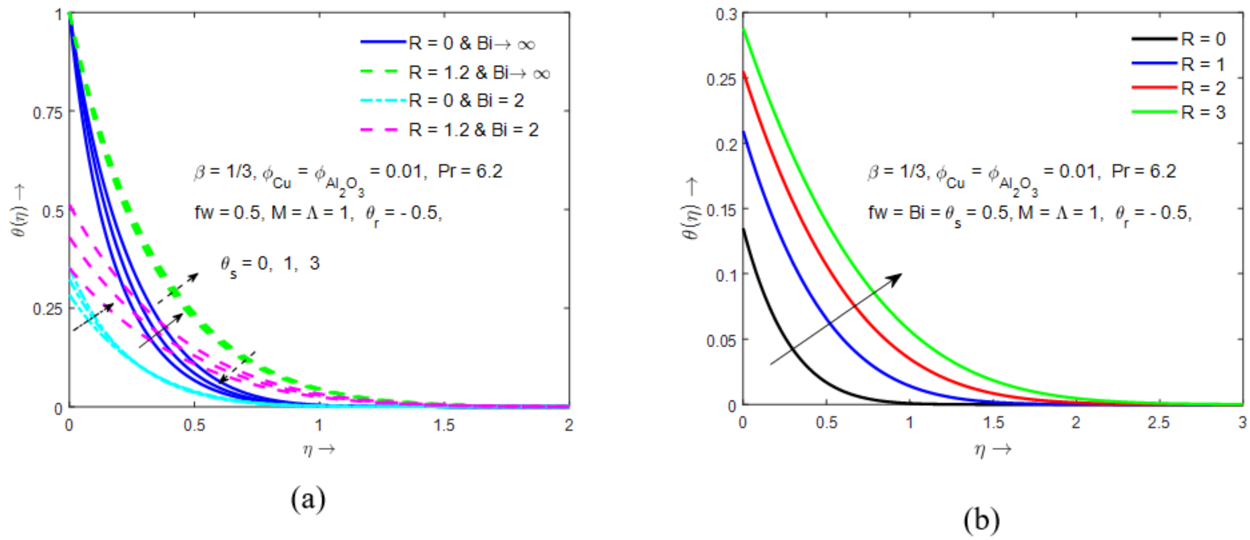

Fig 4. Temperature profiles with respect to θ_s and R

Moreover, $\mathrm{Re}_x{}^{1/2}C_f$ is found to be higher when the fluid has constant viscosity ($\theta_r \to \infty$) compared to when viscosity varies with temperature ($\theta_r = -0.5$), while the reverse trend is observed for $\mathrm{Re}_x{}^{-1/2}\,Nu$. This occurs because temperature-dependent viscosity reduces the effective viscosity near the heated surface, which lowers wall shear stress but intensifies the thermal gradient at the wall, thereby enhancing heat transfer.

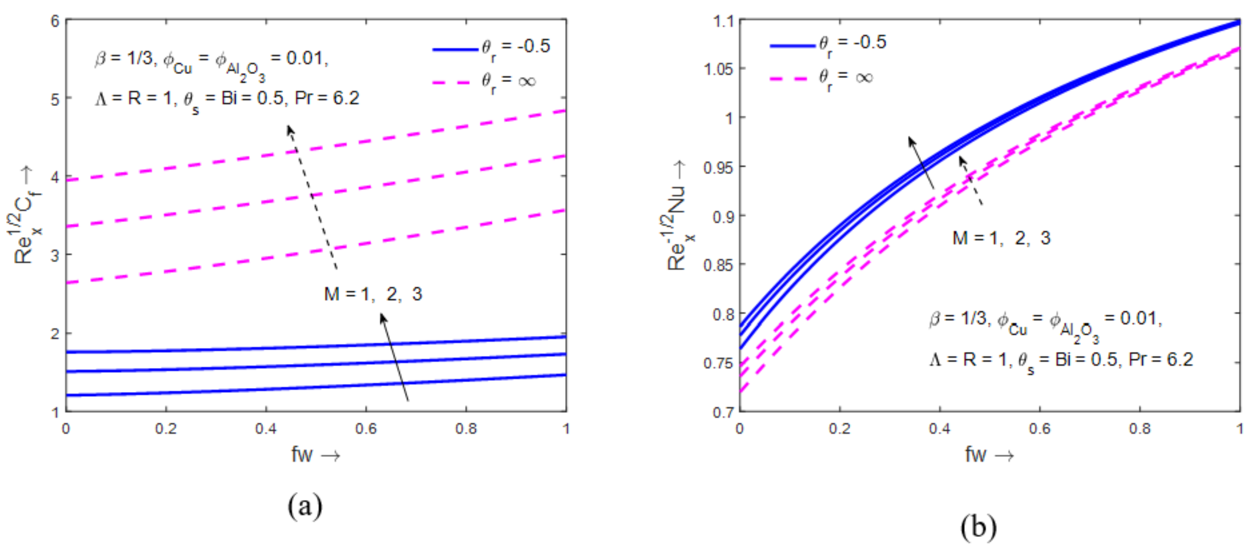

Fig 5. Variation of $\mathrm{Re}_x{}^{1/2}\mathrm{C}_f$ and $\mathrm{Re}_x{}^{-1/2}\mathrm{Nu}$ with f_w for various values of M

4 Conclusion

The current study provides numerical investigations for MHD boundary layer flow of Cu-Al_2O_3/water hybrid nanofluid over a porous wedge under the consideration of variable viscosity and thermal conductivity. The addition of variable fluid properties and convective boundary condition along with thermal radiation effects represents a significant improvement over earlier constant-property models. The key outcomes of the investigation are summarized as follows

- Hybrid nanofluid velocity is higher in the case of variable viscosity compared to constant viscosity, whereas the opposite trend is observed for the temperature profile.
- The variable thermal conductivity parameter (θ_s) increases the fluid temperature when radiation or Biot number act individually. In contrast, under their combined influence, higher θ_s promotes heat dissipation, thereby decreasing the fluid temperature.
- Both local skin friction coefficient and local Nusselt number increase with higher magnetic field strength and suction/injection parameter.
- The hybrid nanofluid increases the local skin friction coefficient because of the elevated effective viscosity and enhanced momentum diffusion compared with single-component nanofluids.
- The hybrid nanofluid also enhances the local Nusselt number when thermal radiation or the Biot number acts individually; however, their combined effect reduces the local Nusselt number compared to the single-component nanofluid.

The current findings can be applied to the design of sophisticated extrusion procedures, cooling and coating systems, targeted drug delivery, and microfluidic devices that utilize hybrid nanofluids to improve heat transport. To further support the theoretical predictions, future studies could examine effects like non-Newtonian hybrid nanofluids, or time-dependent configurations.

5 List of symbols:

Bi: Biot number; C_f: drag friction*;* *K*: thermal conductivity; (B, B_0): variable and constant magnetic field strengths*;* f: dimensionless stream function; M: magnetic parameter*;* f_w: suction/injection parameter; *T*: fluid temperature; *g*: acceleration due to gravity; (*x*, *y*): Cartesian coordinates*;* *m*: constant*;* *Nu*: local Nusselt number; Pr: variable Prandtl number; Pr_{H_2O}: constant Prandtl number*;* q_r: radiative heat flux; *R*: thermal radiation parameter; Re_x: local Reynolds number; T_f: fluid temperature below the surface; T_∞ : ambient temperature; (*u*,v): velocity components*;* *U*: potential flow velocity; V_w: mass suction/injection velocity

Greek symbols- β_T: volumetric coefficient of thermal expansion; β: wedge angle parameter; γ: a constant used in equation (8); δ: a constant used in equation (9); Λ: local buoyancy parameter; σ: electric conductivity; η: similarity variable; τ: shear stress; θ: dimensionless temperature; θ_r: variable viscosity parameter; Ω: total angle of the wedge; μ*:* dynamic viscosity; ν*:* kinematic viscosity; θ_s: variable thermal conductivity parameter; ρ*:* density; ψ*:* stream function;

Subscripts- hnf: hybrid nanofluid; w: surface condition; ∞: ambient condition

Superscripts- $'$: Differentiation with respect to η.

References

1) Parida C, Almubaddel FS, Abdelmohsen SA, Bentalib A, Abdullaeva B, Mohanty D, et al. Numerical analysis of melting heat transfer for radiative and dissipative flow of hybrid nanofluid with entropy optimization. *Journal of the Taiwan Institute of Chemical Engineers*. 2025;175:106271. https://doi.org/10.1016/j.jtice.2025.106271.
2) Anwar MS, Khan M, Hussain Z, Muhammad T, Puneeth V. Investigation of heat transfer characteristics in MHD hybrid nanofluids with variable viscosity and thermal radiations. *Journal of Radiation Research and Applied Sciences*. 2025;18(1):101240. https://doi.org/10.1016/j.jrras.2024.101240.
3) Zainal NA, Nazar R, Naganthran K, Pop I. Stability analysis of unsteady hybrid nanofluid flow over the falkner-skan wedge. *Nanomaterials*. 2022;12(10):1771. https://doi.org/10.3390/nano12101771.
4) Alqahtani AM, Khan W, Smarandache F, Becheikh N, Alroobaea R, Muhammad T. Numerical solution of hybrid nanofluid and its stability over permeable wedge sheet with heat transfer analysis. *IEEE Access*. 2024;12:57633–57645. https://doi.org/10.1109/ACCESS.2024.3378513.
5) Panda S, Ontela S, Thumma T, Mishra SR, Pattnaik PK. Mechanism of heat transfer in Falkner–Skan flow of buoyancy-driven dissipative hybrid nanofluid over a vertical permeable wedge with varying wall temperature. *Modern Physics Letters B*. 2024;38(01):2350211. https://doi.org/10.1142/S0217984923502111.
6) Sharma RP, Badak K, Mishra SR. Investigation of steady viscous magnetohydrodynamic copper–alumina/ethylene glycol hybrid nanofluid in mixed convective vicinity stagnation-point over a vertical plate with Joule heating. *Journal of Thermal Analysis and Calorimetry*. 2024;149(10):4913–4924. https://doi.org/10.1007/s10973-024-13050-6.
7) Mathews J, Hymavathi T. Magnetohydrodynamic stagnation point flow and heat transfer effects of Al2O3-Cu/water hybrid nanofluid over a porous stretching surface. *Proceedings of the Institution of Mechanical Engineers, Part E: Journal of Process Mechanical Engineering*. 2023;237(3):1064–1072. https://doi.org/10.1177/09544089221136692.
8) Ahmed F. Brownian motion's impact on MHD CuO-Al2O3/H2O hybrid nanofluid flow and heat transfer through annular duct. *Proceedings of the Institution of Mechanical Engineers, Part C: Journal of Mechanical Engineering Science*. 2025;239(14):5726–5742. https://doi.org/10.1177/09544062251327842.
9) Alshehry AS, Noor S, Abas SA, Fiza M, Ullah H. Analysis of MHD hybrid nanofluid flow over cone and wedge with exponential and thermal heat source and activation energy. *Open Physics*. 2025;23(1):20250194. https://doi.org/10.1515/phys-2025-0194.

10) Yahaya RI, Arifin NM, Mustafa MS, Pop I, Ali FM, Isa SS. Mixed convection hybrid nanofluid flow past a non-isothermal cone and wedge with radiation and convective boundary condition: Heat transfer optimization. *Case Studies in Thermal Engineering*. 2025;66:105768. https://doi.org/10.1016/j.csite.2025.105768.
11) Pattnaik PK, Mishra SR, Ontela S, Thumma T, Panda S. Exploration of blood flow characteristics on mass-based hybrid ferromagnetic nanofluid with variable magnetized force-driven convective wedge. *Journal of Thermal Analysis and Calorimetry*. 2024;149(15):8493–8504. https://doi.org/10.1007/s10973-024-13057-z.
12) Ogunniyi PO, Gbadeyan AJ, Agarana MC, Yusuf TA. Nonlinear thermal radiation on MHD tangential hyperbolic hybrid nanofluid over a stretching wedge with convective boundary condition. *Heat Transfer*. 2022;51(6):5417–5440. https://doi.org/10.1002/htj.22553.
13) Mandal G, Pal D. Dual solutions of radiative Ag-MoS2/water hybrid nanofluid flow with variable viscosity and variable thermal conductivity along an exponentially shrinking permeable Riga surface: Stability and entropy generation analysis. *International Journal of Modelling and Simulation*. 2024;44(6):360–385. https://doi.org/10.1080/02286203.2023.2171656.
14) Rafique K, Mahmood Z, Muhammad T, Taj M, Alballa T, Khalifa HA. Analyzing the effects of variable fluid properties on radiative dissipative hybrid nanofluid over moving wedge with MHD and Joule heating. *Modern Physics Letters B*. 2025;39(20):2550055. https://doi.org/10.1142/S0217984925500551.
15) Abbas T, Khalil S, Sattar FA. Impact of variable fluid properties and viscous dissipation on hybrid nanofluid (Cu–Al2O3/H2O) flow past a porous stretching sheet. *Multiscale and Multidisciplinary Modeling, Experiments and Design*. 2025;8(7):333. https://doi.org/10.1007/s41939-025-00914-z.
16) Parida P, Swain K, Islahi H. MHD flow and heat transfer of a hybrid nanofluid past a permeable stretching/shrinking wedge. *Optimality*. 2024;1(2):287–299. https://doi.org/10.22105/opt.v1i2.33.
17) Anuar NS, Bachok N, Arifin NM, Rosali H. Analysis of Al2O3-Cu nanofluid flow behaviour over a permeable moving wedge with convective surface boundary conditions. *Journal of King Saud University-Science*. 2021;33(3):101370. https://doi.org/10.1016/j.jksus.2021.101370.
18) Kavitha G, Tankasala V, Vittal C, Dhanalaxmi V, Renuka S. Exploring MHD Effect on Erying-Powell Nanofluid through Porous Media under the Influence of Slips. *Indian Journal of Science and Technology*. 2024;17(32):3281–3295. https://doi.org/10.17485/IJST/v17i32.766.
19) Yahaya RI, Arifin NM, Mustafa MS, Pop I, Ali FM, Isa SS. Mixed convection hybrid nanofluid flow past a non-isothermal cone and wedge with radiation and convective boundary condition: Heat transfer optimization. *Case Studies in Thermal Engineering*. 2025;66:105768. https://doi.org/10.1016/j.csite.2025.105768.
20) Khalil S, Abbas T, Nawaz R. Enhanced thermal and flow behavior of Cu-Al2O3/water hybrid nanofluids in porous media under variable magnetic field conditions. *International Journal of Thermofluids*. 2025;27:101166. https://doi.org/10.1016/j.ijft.2025.101166.
21) Prasad S, Sood S, Chandel S, Sharma D. Impacts of thermal radiation and viscous dissipation on the boundary layer flow of Ferrofluid past a non-flat stretching sheet in a permeable medium: Darcy-Forchheimer's Model. *Indian Journal of Science and Technology*. 2024 2;17(11):990–1002. https://doi.org/10.17485/IJST/v17i11.3027.
22) Ibrahim W, Tulu A. Magnetohydrodynamic (MHD) boundary layer flow past a wedge with heat transfer and viscous effects of nanofluid embedded in porous media. *Mathematical Problems in Engineering*. 2019;2019(1):4507852. http://dx.doi.org/10.1155/2019/4507852.